https://dx.doi.org/10.22161/ijaers.4.10.25 *ISSN: 2349-6495(P) | 2456-1908(O)*

Controller Design of Automatic Guided Vehicle for Path-Following Using Input-Output Feedback Linearization Method

Nguyen Hung

HUTECH Institute of Engineering, HUTECH University of Technology, Vietnam

***Abstract*—** *In this paper, the controller design for path-following using input-output feedback linearization method for the automatic guided vehicle with uncertainties and external disturbances is proposed. The dynamic model of the system with uncertainties and external disturbances is presented. An auxiliary control input vector is designed using input-output linearization technique. The auxiliary control input vector transforms the overall system into two linearized subsystems of the position control subsystem and velocity control subsystem. Based on the two linearized subsystems, a new control law vector for path-following is designed. The new control input vector for path-following guarantees that the tracking errors vector converges exponentially to zero. In addition, a scheme of measuring the errors for experiment by a USB camera is also described. The simulation and experimental results are presented to illustrate effectiveness of the proposed controller.*

***Keywords*—Automatic Guided Vehicle (AGV), Input-Output Feedback Linearization (IOFL), Path-Following Controller (PFC).**

I. INTRODUCTION

Generally, AGV have been used extensively in several industrial and service fields such as transportation, military, security, space, household, office automation and scientific laboratory systems.

Recently, many research results of AGV have been implemented via feedback linearization. In most researches, AGV was considered as a mobile robot. The control problems of a mobile robot include trajectory tracking, to control the robot to follow a desired trajectory starting from a given initial configuration, and point stabilization, to drive a robot from a given initial point to target point. Point stabilization of mobile robot via state-space exact feedback linearization based on dynamic extension approach was proposed in [1]. The objective of this controller is to stabilize a mobile robot at a given target point in the polar coordinate. In [2, 3], feedback linearization technique was also used for trajectory tracking and point stabilization of mobile robot systems. All the above controllers show that they have a good performances and the tracking errors to go to zero in both case but consider only the kinematic model.

Many control schemes have been proposed to deal with the mobile robot control problem including the mechanical system dynamic. In [4], Kalman-based active observer controller (AOB) was applied to the path following. It guarantees the overall system's stability even in the presence of uncertainries. The performance of the proposed control algorithm is verified via simulation results but consider only in discrete model. Jeon et al. [5] also proposed the feedback linearization controller based on dynamic model for lattice type welding with seam tracking sensor that shows a good results in simulation but did not consider uncertainties and external disturbances. Control of welding mobile robot or mobile robot for tracking trajectory considering uncertainties and external disturbances using sliding mode control with good tracking performance are presented in [6]-[9].

This paper proposed the path-following controller design method using input-output feedback linearization technique for the automatic guided vehicle with uncertainties and external disturbances. The dynamic model of the system with uncertainties and external disturbances is presented. An auxiliary control input vector is designed using input-output linearization technique. The auxiliary control input vector transforms the overall system into two linearized subsystems of the position control subsystem and velocity control subsystem. Based on the two linearized subsystems, a new control input vector for path-following is designed. The new control input vector for path-following guarantees that the tracking errors vector converges exponentially to zero. In addition, a scheme of measuring the errors for experiment by a USB camera is also described. The simulation and experimental results are presented to illustrate effectiveness of the proposed controller.

https://dx.doi.org/10.22161/ijaers.4.10.25 *ISSN: 2349-6495(P) | 2456-1908(O)*

II. SYSTEM DESCRIPTION AND MODELING OF AGV

1. System description

Fig. 1 shows configuration of the AGV. It consists of frame, two driving wheels, two passive casters, one rotation wheel, control system and USB camera etc. Fig. 2 shows the configuration for geometric model of the AGV. The two driving wheels are independently driven by two dc motors to achieve a desired motion and orientation. The two driving wheels have the same radius denoted by r and are separated by $2b$. The center of mass of the AGV is located at C; point P is the intersection of a straight line passing through the middle of the vehicle and an axis of the two driving wheels and is rotation center of AGV. The distance between the two points is denoted by d. The body length of the AGV is l. P_a is a tracking point attached to the platform with coordinates (x_a, y_a) and is placed in the X_0 axis at a distance L_a (look-ahead distance) of P. A USB camera is located at the tracking point P_a. The posture of the AGV in the global coordinate frame OXY is specified by the vector $\mathbf{q} = [x_p, y_p, \phi]^T$ where x_p and y_p are the coordinate of point P in the global coordinate frame and ϕ is the orientation of the local frame PX_0Y_0 attached on the AGV platform. The AGV is modeled under the assumptions in [5, 6].

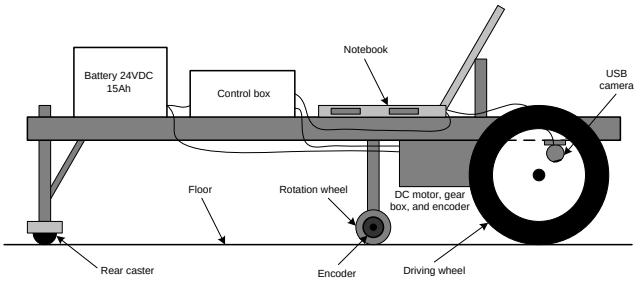

Fig. 1: Configuration of the AGV

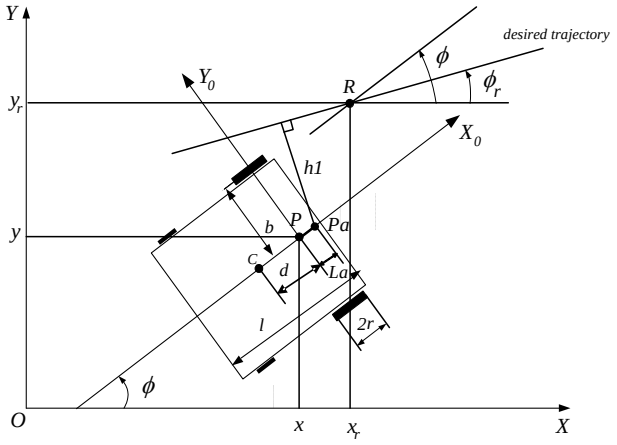

Fig. 2: Configuration for geometric model of the AGV

2. Kinematic Modeling

Consider a robot mobile system having an n-dimensional configuration space with a generalized coordinate vector $\mathbf{q} \in \Re^{n\times 1}$ and the robot is subjected to m independent constraints of the following form [4-[6]:

$$\mathbf{A(q)\dot{q} = 0} \tag{1}$$

where $\mathbf{A(q)} \in \Re^{m\times n}$ is a full rank matrix associated with the nonholonomic constraints.

$\mathbf{S(q)} \in \Re^{n\times(n-m)}$ is defined to be a full rank matrix formed by a set of smooth and linearly independent vector fields, spanning the null space of $\mathbf{A(q)}$. Thus, the result of multiplication of these matrices can be written as follows:

$$\mathbf{A(q)S(q) = 0} \tag{2}$$

Supposing pure rolling conditions with no slip of the wheels, the following kinematics constraints $(m = 3)$ can be written:

$$\dot{x}_p sin\phi - \dot{y}_p cos\phi = 0 \tag{3}$$

$$\dot{x}_p cos\phi + \dot{y}_p sin\phi + b\dot{\phi} = r\dot{\theta}_{rw} \tag{4}$$

$$\dot{x}_p cos\phi + \dot{y}_p sin\phi - b\dot{\phi} = r\dot{\theta}_{lw} \tag{5}$$

From Eqs. (3)-(5), the constraint matrix in Eq. (1) can be obtained as

$$\mathbf{A(q)} = \begin{bmatrix} sin\phi & -cos\phi & 0 & 0 & 0 \\ cos\phi & sin\phi & b & -r & 0 \\ cos\phi & sin\phi & -b & 0 & -r \end{bmatrix} \tag{6}$$

and $\mathbf{q} = \begin{bmatrix} x_p & y_p & \phi & \theta_{rw} & \theta_{lw} \end{bmatrix}^T$ denote configuration of the system $(n = 5)$.

The null space matrix $\mathbf{S(q)}$ of $\mathbf{A(q)}$ that satisfies Eq. (2) is

$$\mathbf{S(q)} = \begin{bmatrix} cb\cos\phi & cb\cos\phi \\ cb\sin\phi & cb\sin\phi \\ c & -c \\ 1 & 0 \\ 0 & 1 \end{bmatrix} \tag{7}$$

where the constant $c = (r / 2b)$.

From the constraint Eq. (1), $\dot{\mathbf{q}}$ must be in the null space of $\mathbf{A(q)}$. It follows that $\dot{\mathbf{q}} \in span\{\mathbf{s_1(q)}, \mathbf{s_2(q)}\}$, and that there exists a smooth angular velocity vector $\mathbf{z} = \begin{bmatrix} \omega_{rw} & \omega_{lw} \end{bmatrix}^T = \begin{bmatrix} \dot{\theta}_{rw} & \dot{\theta}_{lw} \end{bmatrix}^T \in \Re^{(n-m)\times 1}$ such that

$$\mathbf{\dot{q} = S(q)z(t)} \tag{8}$$

where ω_{rw}, ω_{lw} are angular velocities of the right and the left wheels, respectively.

3. Dynamic Modeling

Lagrange equations of motion for the nonholonomic mobile robot system are given by

https://dx.doi.org/10.22161/ijaers.4.10.25 *ISSN: 2349-6495(P) | 2456-1908(O)*

$$\frac{d}{dt}\left(\frac{\partial L}{\partial \dot{q}_k}\right)-\frac{\partial L}{\partial q_k}=f_k-\sum_{j=1}^{m}\lambda_j a_{jk} \tag{9}$$

where λ_j are Lagrange multipliers associated with j^{th} $(j=1,...,3)$ constraint equation, a_{jk} is k^{th} $(k=1,...,5)$ coefficient of k^{th} constraint equation, q_k is generalized coordiate, f_k is generalized force, and L is a Lagrangian. Lagrangian is defined as:

$$L=\frac{m_c}{2}\left(\dot{x}_p^2+\dot{y}_p^2\right)+\frac{m_w}{2}\left(\dot{x}_{rw}^2+\dot{y}_{rw}^2\right)+\frac{m_w}{2}\left(\dot{x}_{lw}^2+\dot{y}_{lw}^2\right)$$
$$+\frac{(I_c+m_c d^2)}{2}\dot{\phi}^2+2\frac{I_m}{2}\dot{\phi}^2+\frac{I_w}{2}\dot{\theta}_{rw}^2+\frac{I_w}{2}\dot{\theta}_{lw}^2 \tag{10}$$

where m_c is the mass of the robot platform and m_w is the mass of each driving wheel plus the rotor of its motor; I_c is the inertia of the robot platform about a vertical axis through the center of mass C; I_w is the inertia of each wheel with the motor's rotor about the wheel axis; and I_m is the inertia about a defined axis in the plan of the wheel (perpendicular to the wheel axis); $(\dot{x}_{rw},\ \dot{y}_{rw})$ and $(\dot{x}_{lw},\ \dot{y}_{lw})$ are linear velocities of right wheel and left wheel in x and y axes, respectively.

Defining $I=I_c+2I_m+2m_w b^2+m_c d^2$ and $m=m_c+2m_w$, Eq. (10) can be rewritten as:

$$L=\frac{m}{2}\left(\dot{x}_p^2+\dot{y}_p^2\right)+\frac{I}{2}\dot{\phi}^2+\frac{I_w}{2}\left(\dot{\theta}_{rw}^2+\dot{\theta}_{lw}^2\right) \tag{11}$$

According to Eqs. (6), (9) and (11), the dynamic model is written as:

$$\begin{aligned}
m\ddot{x}_p &= -\lambda_1\sin\phi-(\lambda_2+\lambda_3)\cos\phi\\
m\ddot{y}_p &= \lambda_1\cos\phi-(\lambda_2+\lambda_3)\sin\phi\\
I\ddot{\phi} &= -(\lambda_2-\lambda_3)b\\
I_w\ddot{\theta}_{rw} &= \tau_{rw}+\lambda_2 r\\
I_w\ddot{\theta}_{lw} &= \tau_{lw}+\lambda_3 r
\end{aligned} \tag{12}$$

where $\lambda_1, \lambda_2, \lambda_3$ are Lagrange multipliers which can effectively be eliminated by the below procedure. τ_{rw} and τ_{lw} are the torques of the right and left wheels, respectively.

The equations in Eq. (12) can be expressed in matrix form, such as:

$$\mathbf{M(q)\ddot{q}+C(q,\dot{q})\dot{q}=D(q)\tau-A^T(q)\lambda} \tag{13}$$

where $\mathbf{M(q)}=\begin{bmatrix} m & 0 & 0 & 0 & 0\\ 0 & m & 0 & 0 & 0\\ 0 & 0 & I & 0 & 0\\ 0 & 0 & 0 & I_w & 0\\ 0 & 0 & 0 & 0 & I_w \end{bmatrix}$,

$\mathbf{C(q,\dot{q})}=\mathbf{O}_{5\times5}$, $\mathbf{D(q)}=\begin{bmatrix} 0 & 0\\ 0 & 0\\ 0 & 0\\ 1 & 0\\ 0 & 1 \end{bmatrix}$, $\boldsymbol{\tau}=\begin{bmatrix}\tau_{rw}\\ \tau_{lw}\end{bmatrix}$.

$\mathbf{M(q)}\in\Re^{n\times n}$ is the inertia matrix; $\mathbf{C(q,\dot{q})}\in\Re^{n\times n}$ is the centripetal and Coriolis forces matrix; $\mathbf{D(q)}\in\Re^{n\times(n-m)}$ is the input transformation matrix; $\mathbf{A^T(q)}\in\Re^{n\times m}$ is a matrix of nonholonomic constraints; $\boldsymbol{\tau}\in\Re^{(n-m)\times1}$ is the control input vector; $\boldsymbol{\lambda}\in\Re^{m\times1}$ is the vector of constraint forces.

4. State Space Realization

Differentiating Eq. (8) with respect to t, substituting in Eq. (13), multiplying the both sides of the equation by $\mathbf{S^T}$ and noticing that $\mathbf{(S^TA^T)\lambda}=0$ from Eq. (2) and $\mathbf{S^TD}=\mathbf{I}_{(n-m)\times(n-m)}$, the following form can be obtained:

$$\mathbf{S^TM\dot{S}\dot{z}+S^T(M\dot{S}+CS)z=\tau} \tag{14}$$

The real dynamic equation of AGV with the external disturbance can be derived from Eq. (14)

$$\begin{aligned}
&\mathbf{S^TM\dot{S}\dot{z}+S^T(M\dot{S}+CS)z+\tau_d=\tau}\\
&\Leftrightarrow \mathbf{\bar{M}\dot{z}+\bar{C}z+\tau_d=\tau}
\end{aligned} \tag{15}$$

where $\mathbf{\bar{M}=S^TMS}\in\Re^{(n-m)\times(n-m)}$,

$\mathbf{\bar{C}=S^T(M\dot{S}+CS)}\in\Re^{(n-m)\times(n-m)}$.

It is assumed that the disturbance vector can be expressed as a multiplier of matrix $\mathbf{\bar{M}}$ as follows [6]:

$$\boldsymbol{\tau}_\mathbf{d}=\mathbf{\bar{M}f}_d\in\Re^{(n-m)\times1},\ \mathbf{f}_d\in\Re^{(n-m)\times1}. \tag{16}$$

$$\mathbf{f}_d=[f_{1d}\ \ f_{2d}]^T,\ |f_{1d}|\le f_{1d}^m,\ |f_{2d}|\le f_{2d}^m. \tag{17}$$

where f_{1d}^m and f_{2d}^m are upper bounds of disturbances.

The state variable vector is defined as

$$\begin{aligned}
\mathbf{x}&=\begin{bmatrix}\mathbf{q} & \mathbf{z}\end{bmatrix}^\mathbf{T}\in\Re^{(2n-m)\times1}\\
&=\begin{bmatrix}x_p & y_p & \phi & \theta_{rw} & \theta_{lw} & \omega_{rw} & \omega_{lw}\end{bmatrix}^T
\end{aligned} \tag{18}$$

Based on Eqs. (8), (15), (16) and (18), the dynamic system of AGV can be expressed in the following state-space form:

$$\dot{\mathbf{x}}=\begin{bmatrix}\dot{\mathbf{q}}\\ \dot{\mathbf{z}}\end{bmatrix}=\begin{bmatrix}\mathbf{Sz}\\ \mathbf{f}_2\end{bmatrix}+\begin{bmatrix}\mathbf{0}_{n\times(n-m)}\\ \mathbf{\bar{M}^{-1}}\end{bmatrix}\boldsymbol{\tau}+\begin{bmatrix}\mathbf{0}_{n\times1}\\ -\mathbf{f}_d\end{bmatrix} \tag{19}$$

where $\mathbf{f}_2=-\mathbf{\bar{M}\bar{C}z}\in\Re^{(n-m)\times1}$.

https://dx.doi.org/10.22161/ijaers.4.10.25 *ISSN: 2349-6495(P) | 2456-1908(O)*

Assuming that the number of system inputs $r \geq (n-m)$, and that $\bar{\mathbf{M}}^{-1}$ has rank $(n-m)$, the following control input vector can be obtained.

$$\boldsymbol{\tau} = \bar{\mathbf{M}}[\mathbf{u} - \mathbf{f}_2 + \mathbf{f}_d] \quad (20)$$

where $\mathbf{u} \equiv \dot{\mathbf{z}} \in \Re^{(n-m)\times 1}$ is an auxiliary control input vector.

From Eq. (20), Eq. (19) can be rewritten to the form

$$\dot{\mathbf{x}} = \begin{bmatrix} \mathbf{S(q)z} \\ \mathbf{0}_{(n-m)\times 1} \end{bmatrix} + \begin{bmatrix} \mathbf{0}_{n\times(n-m)} \\ \mathbf{I}_{(n-m)\times(n-m)} \end{bmatrix} \mathbf{u} = \mathbf{f(x)} + \mathbf{g(x)u} \quad (21)$$

where $\mathbf{f(x)} = \begin{bmatrix} \mathbf{S(q)z} \\ \mathbf{0}_{(n-m)\times 1} \end{bmatrix} \in \Re^{(2n-m)\times 1}$,

$$\mathbf{g(x)} = \begin{bmatrix} \mathbf{0}_{n\times(n-m)} \\ \mathbf{I}_{(n-m)\times(n-m)} \end{bmatrix} \in \Re^{(2n-m)\times(n-m)}.$$

III. CONTROLLER DESIGN FOR PATH-FOLLWING USING INPUT-OUTPUT FEEDBACK LINEARIZATION METHOD

Consider the following MIMO (multi-input/multi-output) nonlinear system.

$$\dot{\mathbf{x}} = \mathbf{f(x)} + \mathbf{g(x)u} \quad (22)$$

$$\mathbf{y} = \mathbf{h(x)} \quad (23)$$

where $\mathbf{x} \in \Re^{(2n-m)\times 1}$ is the state vector, $\mathbf{u} \in \Re^{(n-m)\times 1}$ is auxiliary control input vector, $\mathbf{y} \in \Re^{(n-m)\times 1}$ is the output vector. $\mathbf{f(x)} \in \Re^{(2n-m)\times 1}$ and $\mathbf{g(x)} \in \Re^{(2n-m)\times(n-m)}$ are smooth vector fields, and $\mathbf{h(x)} \in \Re^{(n-m)\times 1}$ are smooth functions on the state space.

The objective of this part is to design a path-following controller that allows the AGV to follow a desired path in the Cartesian space starting from a given initial configuration with a desired linear velocity.

Let the output equation be represented by a vector $\mathbf{y}$ as follows:

$$\mathbf{y} = \begin{bmatrix} y_1 & y_2 \end{bmatrix}^T = \begin{bmatrix} h_1(\mathbf{q}) & h_2(\mathbf{z}) \end{bmatrix}^T \quad (24)$$

where $h_1(\mathbf{q})$ is the shortest distance from the tracking point P_a on the AGV platform to the desired path, $h_2(\mathbf{z})$ is linear velocity v_p of point P of AGV along the X_0 axis.

In case of a straight line described by $Ax + By + C = 0$, the output equations are given as follows:

$$y_1(\mathbf{q}) = h_1(x_a, y_a, \phi) = \left| \frac{Ax_a + By_a + C}{\sqrt{A^2 + B^2}} \right| \quad (25)$$

and $y_2 = h_2(\mathbf{z}) = \dot{x}_p \cos\phi + \dot{y}_p \sin\phi$

$$= \frac{r}{2}(\omega_{rw} + \omega_{lw}) = v_p \quad (26)$$

where (x_a, y_a) is the coordinates of the point P_a; (x_p, y_p, ϕ) is related to the state variables by the following equations.

$$x_a = x_p + L_a \cos\phi \quad (27)$$

$$y_a = y_p + L_a \sin\phi$$

Now, a path-following controller can be designed based on the feedback linearization technique. To get the decoupling matrix for feedback linearization of the above output equations, the output equations are differentiated until the input terms appear in the differentiated output equations as follows:

$$\dot{y}_1 = \frac{\partial h_1}{\partial \mathbf{q}} \dot{\mathbf{q}} = \mathbf{J_{h1}(q)S(q)z} \quad (28)$$

$$\ddot{y}_1 = \frac{\partial(\mathbf{J_{h1}S})}{\partial \mathbf{q}} \dot{\mathbf{q}}\mathbf{z} + \mathbf{J_{h1}(q)S(q)}\dot{\mathbf{z}}$$

$$\Leftrightarrow \ddot{y}_1 = \frac{\partial(\mathbf{J_{h1}S})}{\partial \mathbf{q}} \dot{\mathbf{q}}\mathbf{z} + \mathbf{J_{h1}(q)S(q)u} \quad (29)$$

$$\dot{y}_2 = \mathbf{J_{h2}(z)}\dot{\mathbf{z}} = \mathbf{J_{h2}(z)u} \quad (30)$$

where $\mathbf{J_{h1}(q)} = \frac{\partial h_1}{\partial \mathbf{q}} \in \Re^{1\times n}$ and $\mathbf{J_{h2}(z)} = \frac{\partial h_2}{\partial \mathbf{z}} \in \Re^{1\times(n-m)}$ are Jacobian matrices.

So the decoupling matrix $\mathbf{\Phi_d}$ for the above equations is given as follows:

$$\mathbf{\Phi_d} \equiv \begin{bmatrix} \mathbf{\Phi_{d1}(q)} \\ \mathbf{\Phi_{d2}(z)} \end{bmatrix} \equiv \begin{bmatrix} \mathbf{J_{h1}(q)S(q)} \\ \mathbf{J_{h2}(z)} \end{bmatrix} \in \Re^{2\times(n-m)} \quad (31)$$

where the Jacobian matrices in Eq. (31) for the straight line are calculated from Eqs. (25) and (26) as follows:

$$\mathbf{J_{h1}(q)} = \frac{\partial h_1}{\partial \mathbf{q}}$$

$$= \frac{1}{\sqrt{A^2 + B^2}} \begin{bmatrix} A \\ B \\ BL_a \cos\phi - AL_a \sin\phi \\ 0 \\ 0 \end{bmatrix}^T \quad (32)$$

and $\mathbf{J_{h2}(z)} = \frac{\partial h_2}{\partial \mathbf{z}} = \begin{bmatrix} \frac{r}{2} & \frac{r}{2} \end{bmatrix}$ (33)

The necessary and sufficient condition for the system Eq. (22) to be input-output linearized form and to be controllable is that the determinant of the following decoupling matrix Eq. (31) is not zero, $\det(\mathbf{\Phi_d}) \neq 0$ [8].

$$\det(\mathbf{\Phi_d}) = \frac{r^2 L_a}{2b} \times \frac{(B\cos\phi - A\sin\phi)}{\sqrt{A^2 + B^2}} \quad (34)$$

https://dx.doi.org/10.22161/ijaers.4.10.25 *ISSN: 2349-6495(P) | 2456-1908(O)*

where $\mathbf{\Phi_d}$ is singular if the X_0 axis is perpendicular to the straight line.

From Eqs. (29)-(31), the decoupling matrix is used to establish the input-output feedback linearization as shown below,

$$\ddot{\mathbf{y}} = \begin{bmatrix} \ddot{y}_1 \\ \dot{y}_2 \end{bmatrix} = \dot{\mathbf{\Phi}}_\mathbf{d}\mathbf{z} + \mathbf{\Phi_d}\mathbf{u} \tag{35}$$

where $\dot{\mathbf{\Phi}}_\mathbf{d} = \begin{bmatrix} \frac{\partial(\mathbf{J_{h1}S})}{\partial \mathbf{q}}\dot{\mathbf{q}} \\ \frac{\partial(\mathbf{J_{h2}})}{\partial \mathbf{z}}\dot{\mathbf{z}} \end{bmatrix} = \begin{bmatrix} \frac{\partial(\mathbf{J_{h1}S})}{\partial \mathbf{q}}\dot{\mathbf{q}} \\ \mathbf{0} \end{bmatrix} \in \Re^{2\times(n-m)}$

Assuming that the condition $\det(\mathbf{\Phi_d}) \neq 0$ is satisfied and the transformation of state variables is a diffeomorphism, the auxiliary control input vector for achieving input-output linearization is given by

$$\mathbf{u} = \mathbf{\Phi}_\mathbf{d}^{-1}\left[\boldsymbol{\eta} - \dot{\mathbf{\Phi}}_\mathbf{d}\mathbf{z}\right] \tag{36}$$

where $\mathbf{z}$ is the vector of wheels velocities; $\boldsymbol{\eta} \in \Re^{2\times1}$ is defined as a new control input vector in the following form.

$$\boldsymbol{\eta} = \begin{bmatrix} \eta_1 \\ \eta_2 \end{bmatrix} = \begin{bmatrix} k_P e_p + k_D \dot{e}_p + \ddot{r}_d^1 \\ k_V e_v + \dot{r}_d^2 \end{bmatrix} \tag{37}$$

where a tracking error vector with the position and linear velocity errors is defined as follows:

$$\mathbf{e} = \begin{bmatrix} e_p \\ e_v \end{bmatrix} = \begin{bmatrix} r_d^1 - y_1 \\ r_d^2 - y_2 \end{bmatrix} \tag{38}$$

and k_P, k_D, k_V are gains chosen to ensure the exponential convergence of the control errors to zero; r_d^1, r_d^2 are reference shortest distance and reference linear velocity, respectively.

The new control input vector $\boldsymbol{\eta}$ with $k_P, k_D, k_V > 0$ makes the tracking error vector go to zero.

Subtituting the auxiliary control input vector Eq. (36) into Eq. (35), a closed loop system can be obtained in the following two decoupled linearized form:

$$\begin{bmatrix} \ddot{y}_1 = \eta_1 \\ \dot{y}_2 = \eta_2 \end{bmatrix} \text{ or } \ddot{\mathbf{y}} = \boldsymbol{\eta} \tag{39}$$

Eq. (39) are single input-single output systems with second-order of position control model and first-order of velocity control model.

From Eqs. (37)-(39), the tracking error dynamics of the closed loop systems are given by

$$\ddot{e}_p + k_D\dot{e}_p + k_P e_p = 0 \tag{40}$$

$$\dot{e}_v + k_V e_v = 0 \tag{41}$$

which are exponentially stable [9].

The path-following control scheme is presented in Fig. 3. In Fig. 3, $\mathbf{r_d}$ represents the desired values for the outputs, h_1 and h_2. $\mathbf{e}$ is the error vector between the actual and the desired values. The control input vector Eq. (20) is applied so that the AGV dynamics state equation (19) is simplified into the form Eq. (21). This process is represented by the dotted block in Fig. 3. An auxiliary control input vector Eq. (36) designed with input-output linearization technique linearizes and decouples the overall system into two decoupled linearized subsystems, the position control subsystem and the velocity control subsystem as shown Eq. (39). The thick dashed block in Fig. 3 represents the global system plant with input-output linearization. The new control input vector Eq. (37) makes the tracking error vector go to zezo.

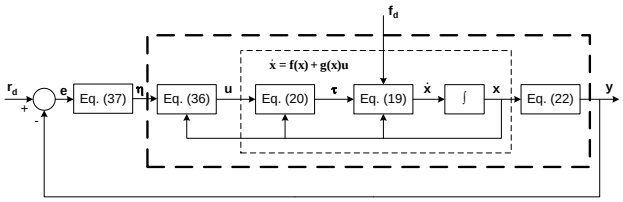

Fig. 3: Scheme of the control algorithm

IV. ERROR MESUREMENT AND HARDWARE

1. Mesurement of tracking error using camera

To achieve the controller, the errors have to be detected. The reference path is a straight line as a desired trajectory marked on a floor. A camera is mounted in front of the AGV to capture directly an image of the tracking line. The errors detecting scheme is shown in Fig. 4.

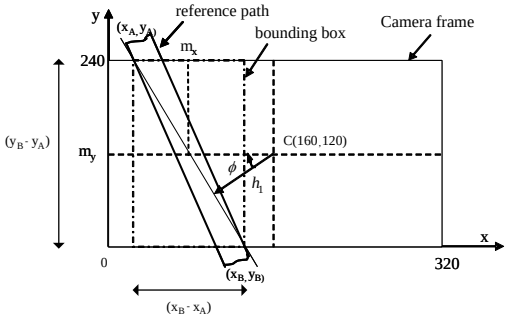

Fig. 4: Errors detecting scheme

The errors can be expressed by

$$\begin{cases} \phi = \arctan[(x_A - x_B)/(y_A - y_B)] \\ h_1 = (160 - m_x)\cos\phi \end{cases} \tag{42}$$

2. Hardware and Control System

The configuration diagram of the total control system is shown in Fig. 5. The control system is based on the integration of notebook and PIC-based controller. The hardware of the system is composed of two-level control: the image processing control as high level computer control and the device control as low level microcontroller control. High-level image processing control algorithms are written in VC++ and run with a sampling time of 15 ms on the notebook (a Pentium IV-

https://dx.doi.org/10.22161/ijaers.4.10.25 *ISSN: 2349-6495(P) | 2456-1908(O)*

2GHz processor). The notebook communicates with the PIC-based controller on the AGV through a COM port.

For the operation, QuickCam SDK is used to capture the image stream into memory in bitmap format with size $320\text{pixel} \times 240\text{pixel}$ via a USB camera at speed of 30 frames per seconds. The image is processed by VC++ program to extract the parameters of bounding box, center and direction of line. These parameters are used to determine oreintation angle and shortest distance as errors detecting scheme in Fig. 4. The input-output feedback linearization controller is designed to calculate the demand velocity of wheels. These demand torques are sent to the PIC-based controller to control the AGV motion. The tracked desired trajectory is shown on the computer interface of image processing in Visual C++ as shown in Fig. 6.

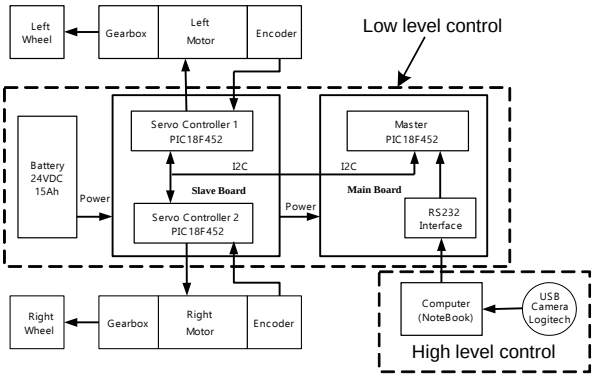

Fig. 5: The configuration of control system

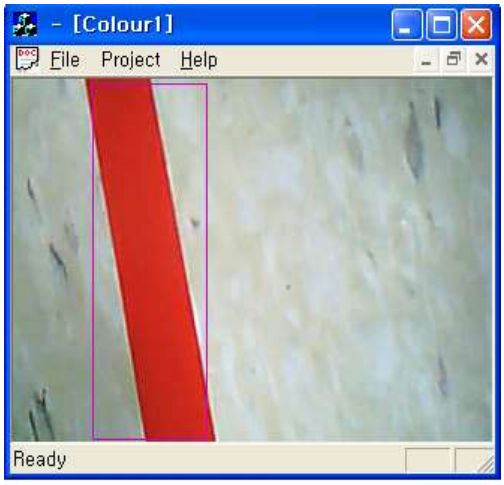

Fig. 6: The tracked desired trajectory

The configuration of the PIC-based controllers for the low level control is shown in Fig. 7. It consists of microcontrollers PIC18F452's which are operated with the clock frequency 40MHz. The microcontroller performs three basis tasks: 1) communicating with the higher-level controller through RS232; 2) reading number of pulses from encoders; and 3) generating PWM duty cycle. The low level controller is composed of two parts: master controller and slave controller. The master controller functions as the low level control, that is, to receive demand velocities from the computer via RS232 and, in turn, to send the commands to the two slave controllers via I2C communication, respectively. The slave controller integrates two PIC18F452's with two motor drivers LMD18200 for the DC motor control. The sampling time of low level control system is about 10ms. The experimental AGV developed for this paper is shown in Fig. 8.

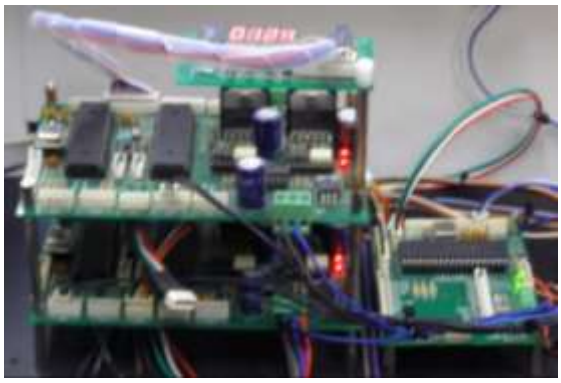

Fig. 7: The configuration of the PIC-based controllers

Fig. 8: The experimental AGV

V. SIMULATION AND EXPERIMENTAL RESULTS

To verify the effectiveness of the proposed controller, simulations have been done for a AGV following a straight line. Fig. 9 shows that the desired trajectory is the straight line of $2.82\,[m]$. The straight line has the form of $y = x$. So the factors are $A = 1, B = -1, C = 0$. The desired linear velocity of AGV is $r_d^2 = 0.05\,[m/s]$. The gains for the new control input vector are $k_P = 3.6\,[s^{-2}]$, $k_D = 1.4\,[s^{-1}]$, $k_V = 4.2\,[s^{-1}]$. The input external disturbances are chosen to be random noises of mean 0 with variance 0.7, and the upper bounds of disturbances are assumed as $f_{1d}^m = 1\,[rad/s^2]$ and $f_{2d}^m = 1\,[rad/s^2]$. The numerical parameter values and the innital values for

https://dx.doi.org/10.22161/ijaers.4.10.25 *ISSN: 2349-6495(P) | 2456-1908(O)*

simulation and experiment are given in Table 1 and Table 2.

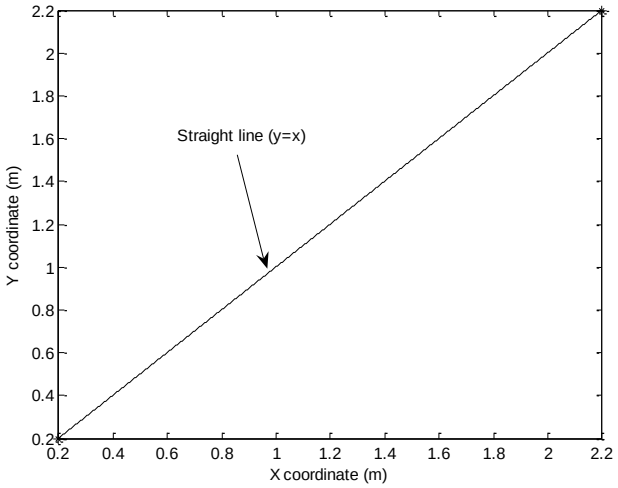

Fig. 9: The desired trajectory

Table. 1: The numerical parameters values for simulation and experiment

Parameters	Values	Units
b	0.39	$[m]$
r	0.16	$[m]$
d	0.45	$[m]$
l	1.2	$[m]$
m_c	32.67	$[kg]$
m_w	2.75	$[kg]$
I_c	17.85	$[kgm^2]$
I_w	0.0135	$[kgm^2]$
I_m	0.0068	$[kgm^2]$

Table. 2: The initial values for simulation and experiment

x_r	0.2 $[m]$	x_p	0.32 $[m]$
y_r	0.2 $[m]$	y_p	0.24 $[m]$
ϕ_r	45 [deg]	ϕ	30[deg]
v_p	0 $[m/s]$	Reference inputs	$r_d^1 = 0\,[m]$, $r_d^2 = 0.05\,[m/s]$
L_a	0.06 $[m]$	Sampling time	$\Delta T = 0.01\,[s]$

The simulation and experimental results for path-following are shown in Figs. 10 to 17. Figs. 10 and 11 show the movement of the AGV along the desired trajectory for full time 40 seconds and the beginning time. As shown in Fig. 12, the tracking point P_a of the AGV is able to reach the straight line path and stay on the path for full time. Fig. 13 shows that the linear velocity of the AGV is at the vicinity of $0.05\,[m/s]$ as desired. The experimental position error e_p and the experimental linear velocity error e_v converge to zero and are bounded along the simulation result as shown in Figs. 14 and 15. The angular velocities of left and right wheel are shown in Fig. 16. It shows that the angular velocities of left and right wheels change quickly at the beginning time and have same value about $0.32\,[rad/s]$ for following the straight line from about 7 seconds. Fig. 17 shows the control input vector $\boldsymbol{\tau}$. They change greatly at the beginning time. However, they are bounded within the bounds of $\pm 7.6\,[N.m]$ and their average value converges to zero when AGV moves along the desired trajectory after 4 seconds. The above simulation and experimental results are presented to illustrate the effectiveness of the proposed control algorithm.

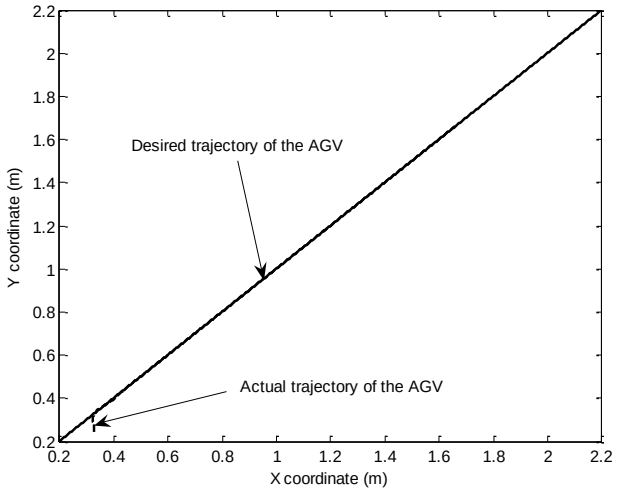

Fig. 10: Movement of AGV for full time

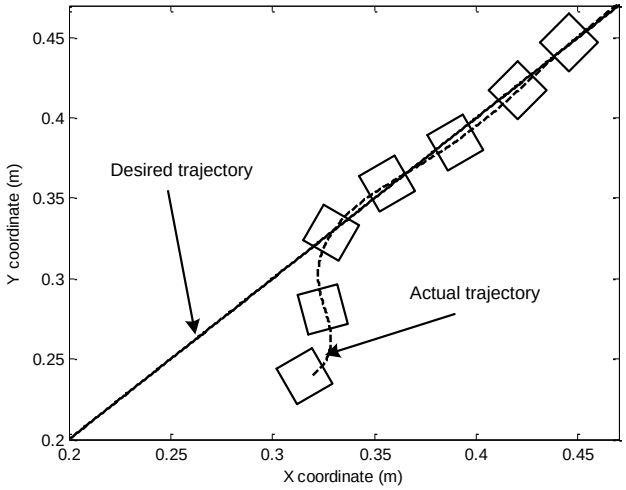

Fig. 11: Movement of AGV at the beginning time

https://dx.doi.org/10.22161/ijaers.4.10.25 *ISSN: 2349-6495(P) | 2456-1908(O)*

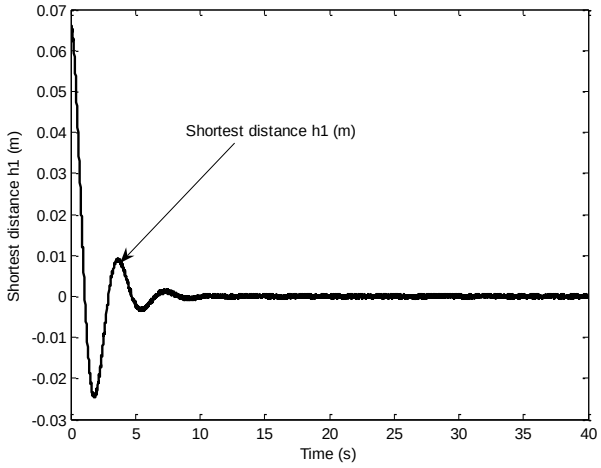

Fig. 12: Shortest distance h_1

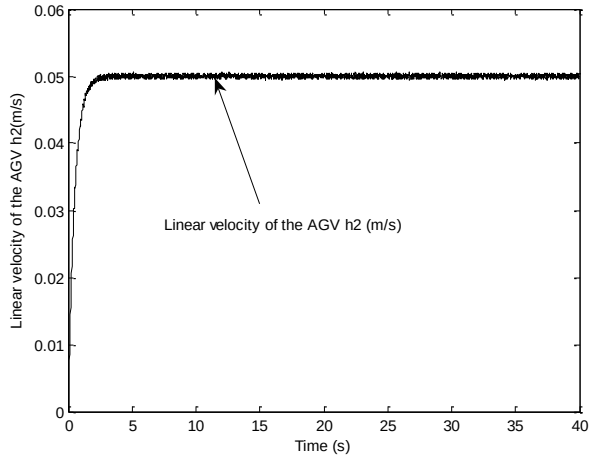

Fig. 13: Linear velocity of the AGV for full time

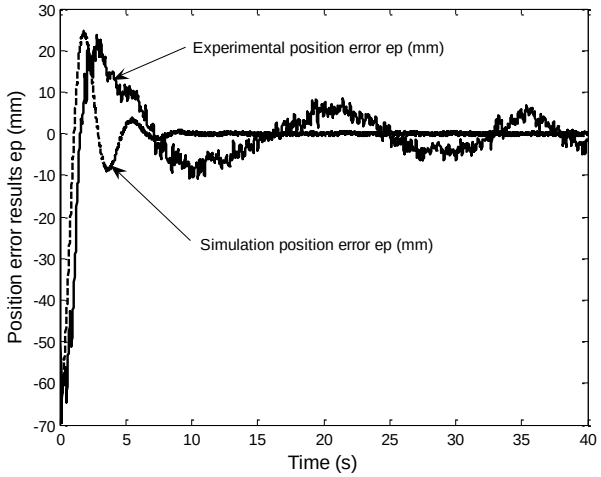

Fig. 14: Simulation and experimental position error results e_p

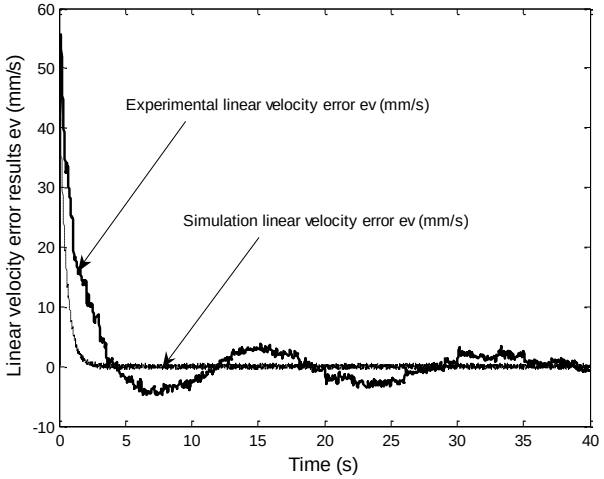

Fig. 15: Simulation and experimental linear velocity error results e_v

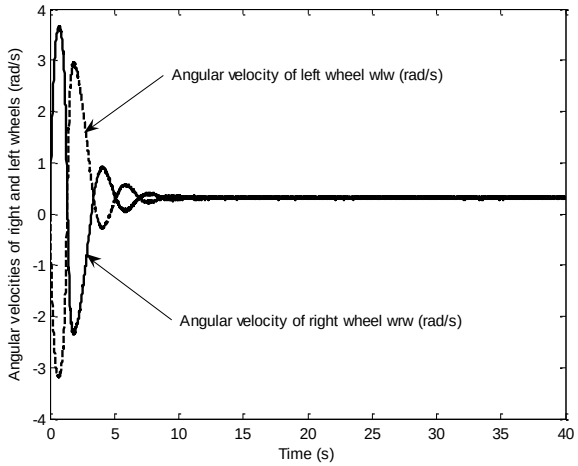

Fig. 16: Angular velocities of the right and left wheels

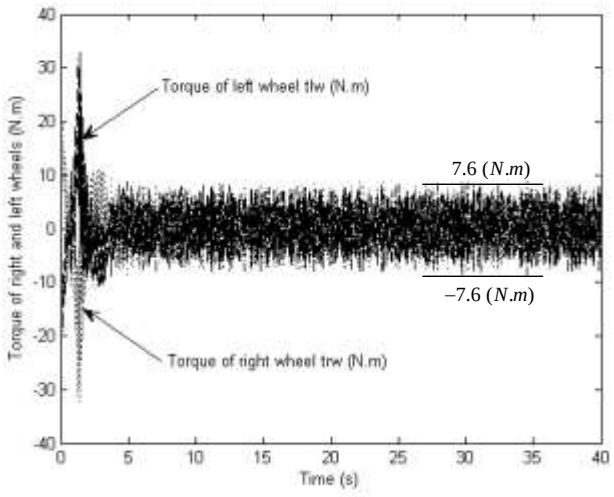

Fig. 17: Control input vector $\boldsymbol{\tau}$

VI. CONCLUSION

In this paper, a path-following controller is proposed based on the dynamic model of AGV under uncertainties and external disturbances using input-output feedback linearization method. Using the input-output feedback

https://dx.doi.org/10.22161/ijaers.4.10.25 *ISSN: 2349-6495(P) | 2456-1908(O)*

linearization technique, two decoupled linearized SISO system are obtained: a second-order position model, and a first-order velocity model. A new control input vector is chosen to make the tracking error vector go exponentially to zero. To implement the proposed controller, a control system is developed based on PIC microcontroller and USB camera. The simulation and experimental results are presented to illustrate the good applicability to AGV of the proposed control algorithm.

REFERENCES

[1] K. C. Park, H. Chung and J. G. Lee (2000). Point stabilization of mobile robots via state-space exact feedback linearization. Robotics and Computer-Integrated Manufacturing (ISSN: 0736-5845), 16(5), 353-363.

[2] S. Sun and P. Cui (2004). Path tracking and a practical point stabilization of mobile robot. Robotics and Computer-Integrated Manufacturing (ISSN: 0736-5845), 20(1), 29-34.

[3] G. Oriolo, A. De Luca and M. Vendittelli (2002). WMR control via dynamic feedback linearization: Design, implementation and experimental validation. IEEE Trans. on Control Systems Technology (ISSN: 1063-6536), 10(6), 835-852.

[4] P. Ceolho and U. Nunes (2005). Path following control of mobile robots in presence of uncertainties. IEEE Trans. on Robotics (ISSN: 1552-3098), 21(2), 252-261.

[5] Y. B. Jeon, S. B. Kim and S. S. Park (2002). Modeling and motion control of mobile robot for lattice type welding. KSME International Journal (ISSN: 1738-494X(P) | 1976-3824(O)), 16(1), 83-93.

[6] N. M. Dung, V. H. Duy, N. T. Phuong, S. B. Kim and M. S. Oh. Two-wheeled welding mobile robot for tracking a smooth curved welding path using adaptive sliding-mode control technique (2007). International Journal of Control, Automation, and Systems (ISSN: 1598-6446 (P) | 2005-4092 (O)), 5(3), 283-294.

[7] T. L. Chung, T. H. Bui, T. T. Nguyen, S. B. Kim (2004). Sliding Mode Control of Two-Wheeled Welding Mobile Robot for Tracking Smooth Curved Welding Path. KSME International Journal (ISSN: 1738-494X(P) | 1976-3824(O)), 18(7), 1904-1106.

[8] J. M. Yang, J. H. Kim (1999). Sliding mode control for trajectory tracking of nonholonomic wheeled mobile robots. IEEE Trans. on Robotics and Automation (ISSN: 1042-296X), 15(3), 578-587.

[9] N. Hung, Tuan. D. V, Jae. S. I, H. K. Kim, S. B. Kim (2010). Motion Control of Omnidirectional Mobile Platform for Trajectory Tracking Using Integral Sliding Mode Controller. International Journal of Control, Automation, and Systems (IJCAS) (ISSN : 1598-6446 (P) | 2005-4092 (O)), 8(6), 1221-1231.

[10] H. Nijmeijer and A. Schaft (1990). Nonlinear Dynamic Control System, New York: Springer-Verlag.

[11] J. J. E. Slotine and W. Li (1991). Applied Nonlinear Control, Prentice-Hall International, Inc.